Pol. J. Environ. Stud. Vol. 34, No. 4 (2025), 4833-4842
DOI: *10.15244/pjoes/188595* ONLINE PUBLICATION DATE: 2025-05-05

Original Research

Polyethyleneimine-Modified Garden Waste Biochar: Preparation and Its Application for Aqueous Cr(VI) Adsorption

Mihua Wei[1, 2], Yang Shao[3], Xiaohan Duan[1,4], Jingxi Tie[3]*

[1]School of Water Conservancy, North China University of Water Resources and Electric Power, Zhengzhou 450046, PR China
[2]Henan Key Laboratory of Water Resources Conservation and Intensive Utilization in the Yellow River Basin, Zhengzhou, 450046, PR China
[3]School of Environmental and Municipal Engineering, North China University of Water Resources and Electric Power, Zhengzhou, 450046, PR China
[4]Henan Vocational College of Water Conservancy and Environment, Zhengzhou 450008, PR China

Received: 25 September 2023
Accepted: 12 May 2024

Abstract

Garden Waste (GW) and Polyethyleneimine were used as source materials to create polyethyleneimine-modified garden waste biochar (PGWBC). The composite was employed as an adsorbent in both static and dynamic Cr(VI) adsorption experiments after being evaluated using N_2 adsorption-desorption and Fourier transform infrared spectroscopy. The material characterization results indicated that PGWBC was a mesoporous material that contained mainly narrow slit mesopores. The static adsorption data indicated that Cr(VI) adsorption by PGWBC was a pH-dependent process, a rise in pH from 2 to 9 resulting in a decrease in Cr(VI) adsorption from 44.6 mg/g to 3.8 mg/g. The adsorption process was endothermic and spontaneous, as characterized by the pseudo-second-order model and the Langmuir equation, the maximum Cr(VI) uptake was 56.1 mg/g in 308 K. The dynamic adsorption revealed that increasing the flow rate impaired Cr(VI) adsorption, and the Thomas model was more suited to represent Cr(VI) adsorption by PGWBC than the Yoon-Nelson model.

Keywords: garden waste, polyethyleneimine, biochar, Cr(VI) adsorption

Introduction

As a heavy metal, chromium (Cr) is widely used in a large variety of industries, such as textile mills, electroplating plants, wood mills, and tanneries [1, 2]. Take the chromium-rich tannery wastewater as an example, the concentration of Cr varies greatly due to the different processes and the amount of chemicals used, which are mostly distributed in the range of 0.2 - 247 mg/L based on previous studies [3-7]. Maximum permissible limits of total Cr for drinking water are 0.1 mg/L and 0.05 mg/L according to the United States Environmental Protection Agency (USEPA) and World Health Organization (WHO), respectively [8]. As the dominating existing form of Cr, Cr(VI) in the wastewater discharged from the industries can cause substantial

*e-mail: 15202843@qq.com

harm to aquatic creatures and human health due to its carcinogenic, teratogenic, and mutagenic nature [9]. As a result, Cr(VI)-bearing wastewater must be purified before being discharged into the environment.

Various techniques, including adsorption [10], membrane filtration [11], electrocoagulation [12], ion exchange [13], and other approaches have been investigated for Cr(VI)-bearing wastewater purification [14]. Among the techniques listed above, adsorption has attracted particular attention because of its merits, including low cost, easy operation, and high performance, etc. [15].

According to previous studies, biochars generated from diverse raw materials have been applied for Cr(VI) removal successfully due to their merits of a wide range of raw materials, easy preparation, and effective Cr(VI) removal performance [16-19]. Several strategies have been used to alter biochar in order to increase its Cr(VI) removal. For instance, Wang et al. prepared sludge-based biochar (SBC), KOH-activated SBC (SBC-KOH), and nano-zero-valent iron-supported SBC-KOH (nZVI@SBC-KOH). The Cr(VI) removal rates of the three materials were 34.83%, 61.58%, and 99.36%, respectively [20]. Shi et al. modified the biochar derived from glue residue with HCl, $ZnCl_{2,}$ and KOH, and the research showed that all the three modified biochars performed better than the raw biochar for Cr(VI) removal [21]. Amino compounds [22] have received a lot of attention among the modifiers because they can greatly increase the Cr(VI) removal of biochar by strong electrostatic attraction between the Cr(VI) oxyanion and the protonated amine, formation of chelate between Cr(VI) and basic amine groups and reduction of Cr(VI) to Cr(III) with lower toxicity by amine groups [23, 24]. Deng et al. modified Camellia oleifera shell-based biochar with acrylamide and dimethyldiallyl ammonium chloride to significantly increase its Cr(VI) removal from 36.4 to 394.0 mg/g [25].

The growing urbanization in China generates a tremendous amount of GW. Currently, GW is mostly disposed of through incineration, landfill and biodegradation, all of which need a lot of space, cost a lot of money, and harm the environment [26]. GW has been shown to be an excellent feedstock for the production of biochar. Zhang et al. found that biochars made from six different types of garden waste had Cr(VI) adsorption values ranging from 32.7 to 51.4 mg/g [27].

In this study, we prepared a garden waste biochar (GWBC) and modified it with polyethyleneimine (PEI) to get PGWBC [28]. The prepared composite was used as an adsorbent to conducted both static and dynamic tests to explore its Cr(VI) adsorption performance.

Materials and Methods

Adsorbent Preparation

The GW used in this study was gathered from the community for a university's teaching faculty in Zhengzhou, China. The GW is primarily composed of grass (*Lolium perenne L.*) and the leaves of osmanthus (*Osmanthus fragrans* (*Thunb.*) *Lour.*). The GW was dried in the open air for days and at 105°C for 2 h before being crushed and processed through 0.15 mm mesh. We prepared the GWBC by Pyrolysis, 15 g of GW powder was placed in a tube furnace and heated to 500-1000°C (GWBC500-GWBC1000) at a rising gradient of 15°C/min for 2-6 h, respectively. By adding N_2 to the furnace at a rate of 20 mL/min, an atmosphere free of oxygen was formed. After cooling, the black particles were broken up and put through a 0.18 mm screen to create GW biochar (GWBC).

20 mL of the PEI and methanol combination (m:m = 1:100, 1:20, and 1:10) with the mass fractions of 1%, 5% and 10% was mixed with GWBC in a range of ratios (W:V=0.1:20, 0.5:20, 1:20, 1.5:20, and 2:20), and the mixture was vigorously stirred for 5 h at 30°C. To get the PEI modified GWBC (PGWBC), the solids were filtered, washed with deionized water until the pH was constant, and then vacuum-dried for 4 h at 60°C.

Adsorbent Characterization

A Fourier transform infrared spectroscopy (FTIR, Nicolet IS50, Thermo fisher, USA) was used to analyze the functional groups of PGWBC before and after Cr(VI) adsorption. An automatic specific surface area analyzer (BELSORP-max, MicrotracBEL, Japan) was utilized to measure the specific surface area and pore features of PGWBC.

Artificial Wastewater Synthesis

The wastewater containing Cr(VI) was synthesized by dissolving a certain amount of $K_2Cr_2O_7$ into the deionized water. The pH value of the working solution was adjusted using dilute HCl and NaOH solutions.

Batch Adsorption Experiment

0.02 g PGWBC was added into 50 mL Cr(VI)-bearing wastewater, and the mixture was incubated in a shaker at 120 rpm, reacting at different time spans and temperatures. The residual Cr(VI) in the supernatant was determined by a UV-vis spectrophotometer (UV-5100, Yuanxi, China) using the 1,5-diphenylcarbazide method at 540 nm [29]. All the experiments were carried out in triplicate.

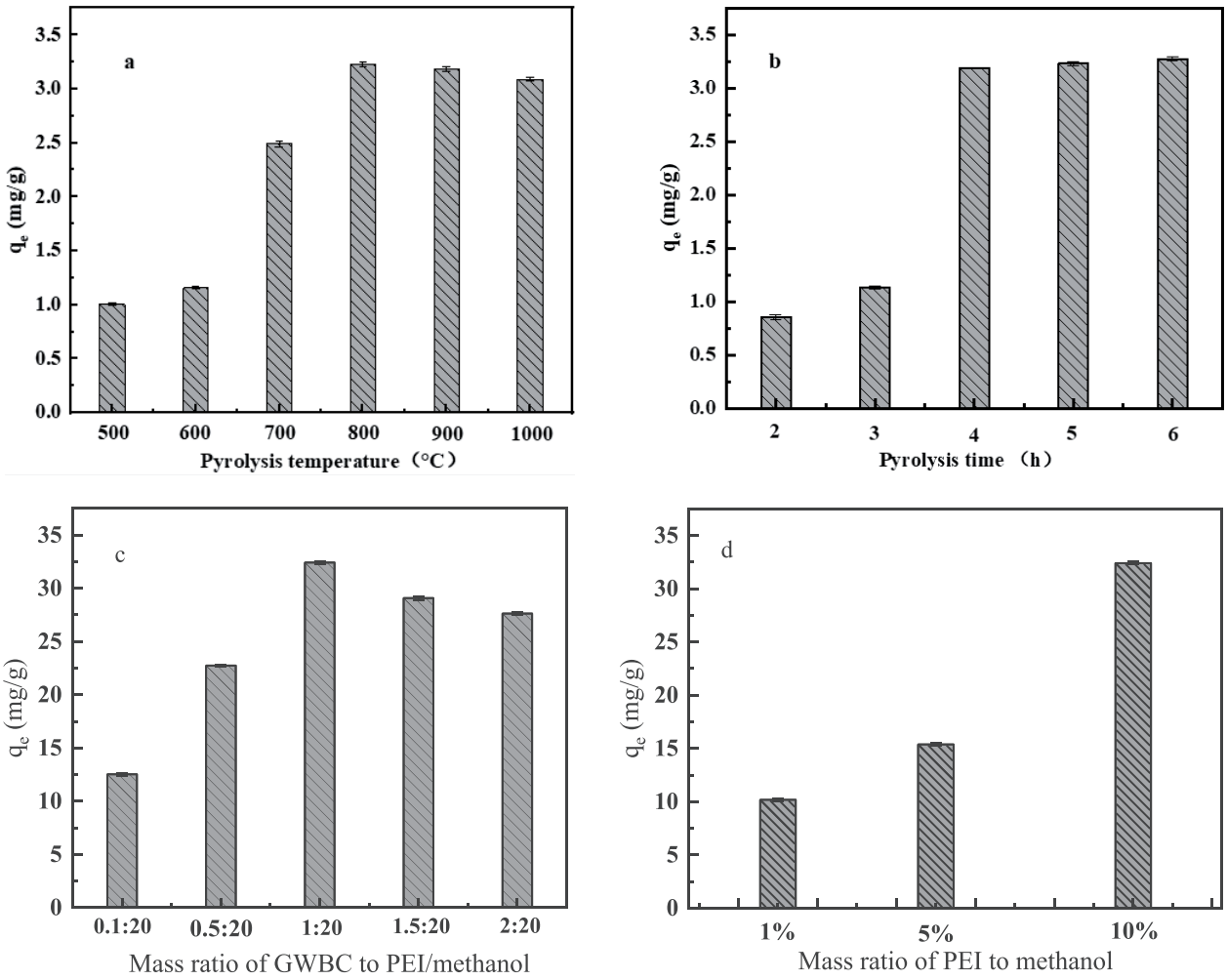

Fig. 1. Investigation of the optimal conditions for PGWBC preparation based on the Cr(VI) adsorption: determination of the optimal temperature (a) (T=298 K, t=4 h,C_0=50 mg/L); determination of the optimal pyrolysis time for GWBC preparation (b) (T=298 K, C_0=50 mg/L); determination of optimal GWBC:(PEI/methanol) (m:m) (c) (T=298 K, t=4 h,C_0=50 mg/L); determination of the optimal mass ratio of PEI:methanol (m:m) (d) for PGWBC preparation (T=298 K, t=4 h, C_0=50 mg/L).

Results and Discussion

Investigation of the Optimal Condition for PGWBC Preparation

As shown in Fig. 1a, 800 °C was determined as the optimal temperature due to the fact that GWBC800 had the highest Cr(VI) uptake of 3.23 mg/g in the temperature range of 500-1000 °C. Cr(VI) uptake rose from 0.85 mg/g to 3.18 mg/g as the pyrolysis time increased from 2 to 4 h, and continued to increase to 3.22 mg/g marginally when the pyrolysis time increased to 6h (Fig. 1b). Hence, 4h was determined as the best pyrolysis time for GWBC preparation considering the energy conservation. The ratio of GWBC:(PEI/methanol) (m:m) =1:20 was best since PGWBC prepared at the condition had the largest Cr(VI) uptake of 32.42 mg/g (Fig. 1c), which was better the other two composites prepared using the mass fractions of 1% and 5% (Fig. 1d). According to the above description, the optimal condition for PGWBC preparation was that GWBC created at 800°C for 4 h was reacted with a combination of PEI and methanol (m_{PEI}:$m_{methanol}$=1:10) at 1:20 (m_{GWBC}:$m_{PEI/methanol}$) , which was used to prepare the PGWBC for the following studies.

Characterization

As shown in Fig. 2, both GWBC and PGWBC possessed type IV adsorption-desorption isotherm with type H_4 hysteresis loop, indicating the two materials contained mainly narrow slit mesopores. GWBC and PGWBC had pore size distribution in the range of 0.91-1.86 nm and 0.68-1.99 nm, respectively, and their corresponding peaks were located at around 1.30 nm and 1.12 nm, respectively, indicating the two biochars were mesoporous materials.

As shown in Table 1, PGWBC had a much larger BET specific area and total pore volume than those of GWBC due to the PEI modification, offering more active sites for better Cr(VI) adsorption [30], whereas, PGWBC had less average pore diameter than GWBC,

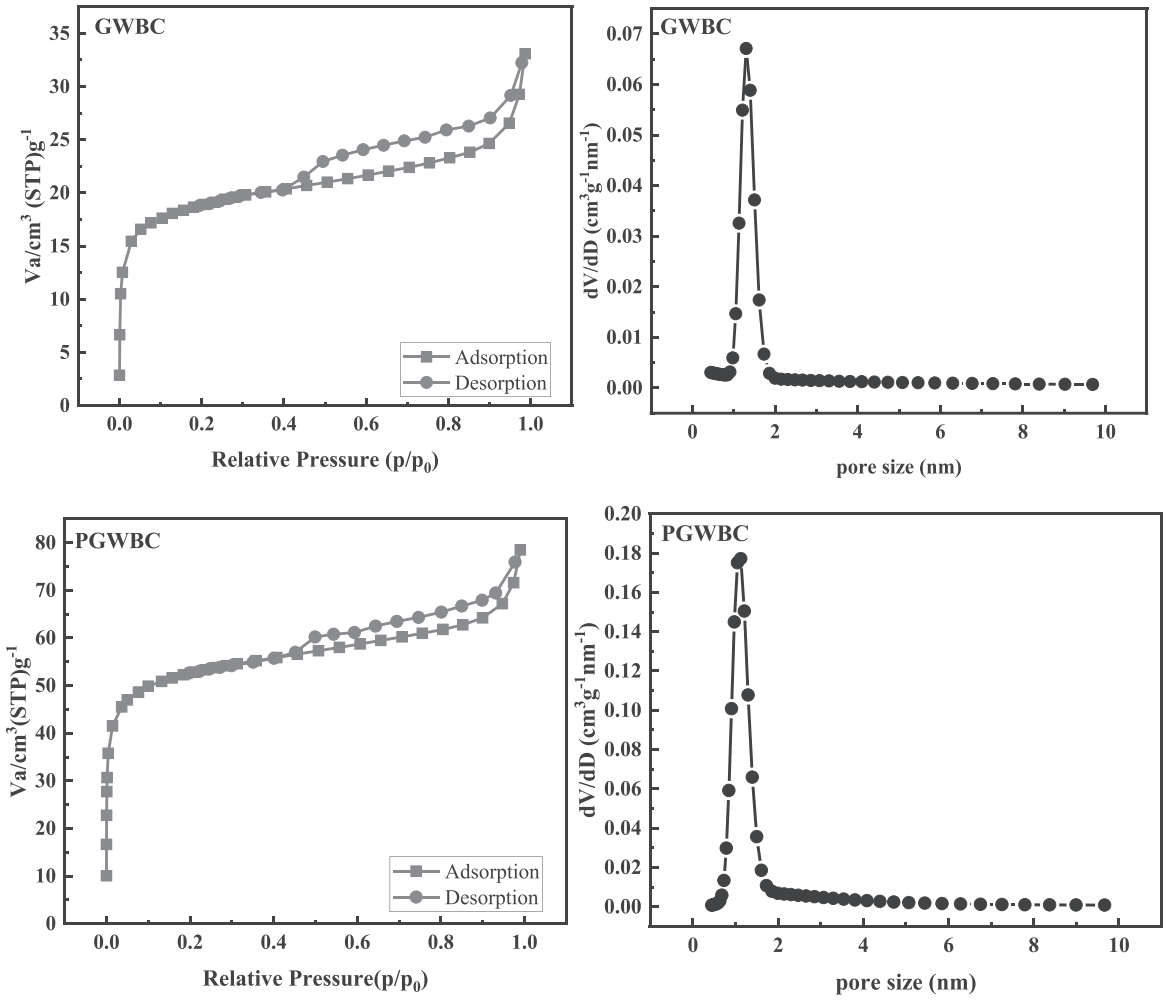

Fig. 2. Nitrogen adsorption-desorption isotherms and pore size distribution of GWBC and PGWBC.

Table 1. Specific surface areas and pore textures of GWBC and PGWBC.

Sample	S_{BET} (m^2/g)	V_{tot} (cm^3/g)	Average pore diameter (nm)
GWBC	69.34	0.05	2.95
PGWBC	198.41	0.21	2.44

which might have been caused by the blocking of the pore by PEI [31].

In contrast to that of GWBC (Fig. 3a), the FTIR spectra of PGWBC (Fig. 3b) showed the NH_2 stretching at 3432 and 1636 cm^{-1} [32, 33], respectively, and CN stretching at 1384 cm^{-1} [34], indicating the surface of GWBC was successfully modified by PEI.

Static Adsorption

Effect of Initial Solution pH

pH played a very important role in Cr(VI) adsorption [35]. As shown in Fig. 4a, Cr(VI) uptake by PGWBC dcreased from 44.6 mg/g to 3.8 mg/g as the solution pH rose from 2 to 9, indicating lower pH was better for Cr(VI) adsorption because Cr(VI) existed primarily in the forms of oxyanions with negative charges, which competed with OH^- for the active sites with rising pH, leading to a decreasing Cr(VI) adsorption. Meanwhile, as shown in Fig. 4b, pH_{pzc} of PGWBC was at around pH=3.19, resulting in the negatively charged surface at pH>3.19, which also decreased Cr(VI) adsorption.

Kinetic Study

As shown in Fig. 5, Cr(VI) uptake rose rapidly with the increase of reaction time during the first 240 min for both of the two different initial Cr(VI) concentrations due to there being enough free active sites on the surface of PGWBC for swift Cr(VI) adsorption, and about 76.7% and 85.6% of total Cr(VI) were removed

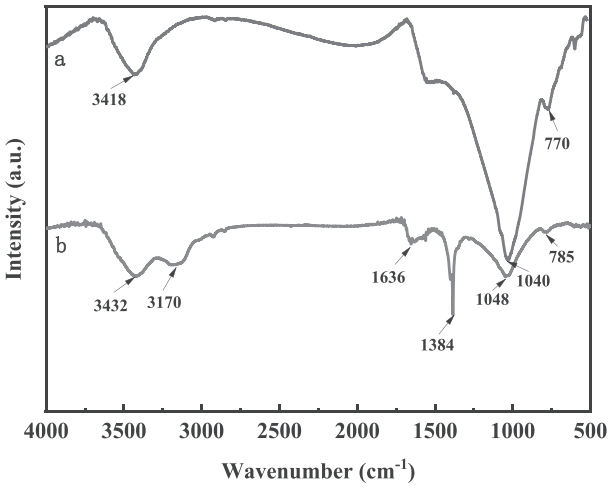

Fig. 3. FTIR spectra of GWBC (a) and PGWBC (b).

during this stage for the two reactions, respectively. In the subsequent stage, the reaction was slowed down as the active sites decreased.

The pseudo-first-order model, the pseudo-second-order model, and the Elovich model (1-3) were used to further investigate the experiment data [36-38].

$$\log(q_e - q_t) = \log q_e - \frac{k_1}{2.303} t \quad (1)$$

$$\frac{t}{q_t} = \frac{t}{q_e} + \frac{1}{k_2 q_e^2} \quad (2)$$

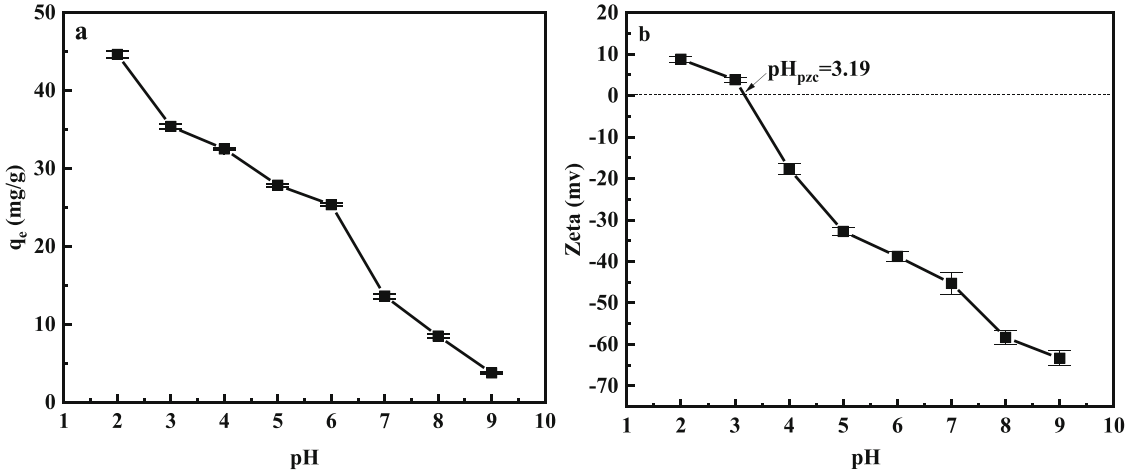

Fig. 4. Influence of the initial solution pH on the adsorption of Cr(VI) (a), Zeta potential analysis of PGWBC (b).

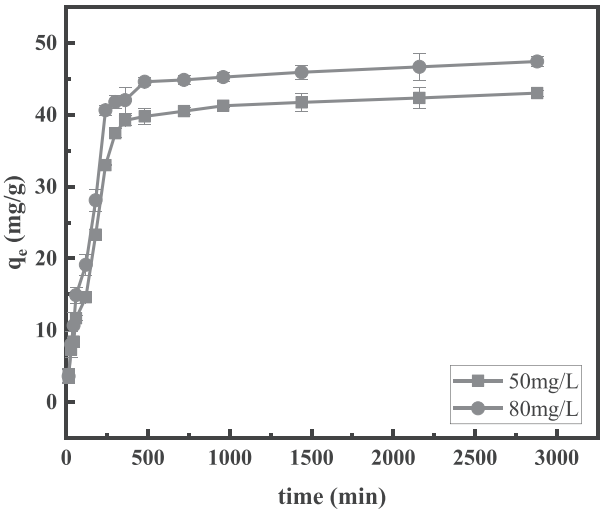

Fig. 5. Effect of contact time on Cr(VI) adsorption (m=0.02 g, pH=4, T=298 K).

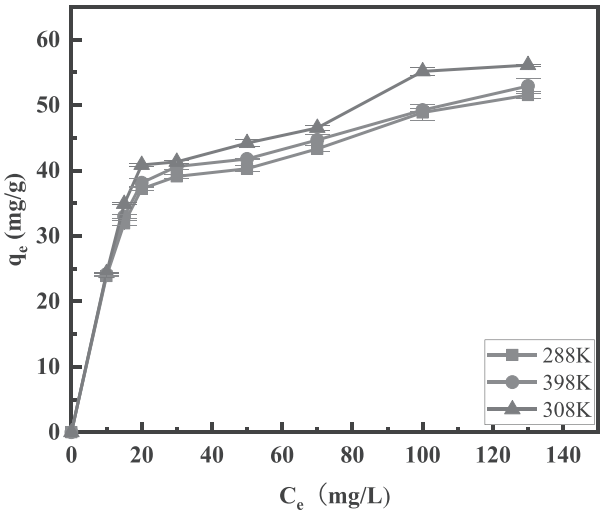

Fig. 6. The isotherms of Cr(VI) adsorption by PGWBC at different temperatures (m=0.02g, pH=4, t=48h).

Table 2. Kinetic parameters of Cr(VI)adsorption by PGWBC.

C_0 mg/L	Pseudo-first order			Pseudo-second order			Elovich		
	q_e (mg/g)	k_1 (min-1)	R^2	q_e (mg/g)	k_2 [g/(mg·min)]	R^2	α [g/(mg·min)]	β (g/mg)	R^2
50	19.53	0.0027	0.8113	44.33	0.000178	0.9951	94.36	0.113	0.8788
80	22.33	0.0019	0.7928	49.65	0.000173	0.9974	81.98	0.106	0.8831

Table 3. Isotherm parameters of Cr(VI) adsorption by PGWBC at different temperatures.

Temperature (K)	Langmuir				Freundlich		
	q_m (mg/g)	K_L (L/mg)	R^2	R_L	K_F (mg/g)	n	R^2
288	51.1771	0.2719	0.9911	0.0275	28.4085	8.3724	0.9573
298	52.1105	0.3028	0.9917	0.0248	29.9659	8.8394	0.9605
308	56.0852	0.2919	0.9895	0.0257	31.8654	8.7207	0.9176

$$q_t = \frac{1}{\beta}\ln(\alpha\beta) + \frac{1}{\beta}\ln t \tag{3}$$

Where q_e (mg/g) and q_t (mg/g) were the Cr(VI) uptake at equilibrium and time t, respectively; k_1 (min^{-1}) and k_2 (g/mg·min) were the rate constants for the pseudo-first-order model and the pseudo-second-order model, respectively; α (mg/g·min) was the Elovich adsorption rate, and β (g/mg) was the Elovich constant.

Table 2 showed the kinetic parameters of the three kinetic models. The R^2 of the pseudo-second-order model was much higher than those of the other two models, and the calculated Cr(VI) uptake at equilibrium (44.33 mg/g for C_0=50 mg/L, 49.65 mg/g for C_0=80 mg/L) was close to the experimental values, indicating the pseudo-second-order model was best to describe the adsorption process.

Isotherm and Thermodynamic Study

Fig. 6 showed the residual Cr(VI) in the solution and the Cr(VI) adsorption by PGWBC at equilibrium. Two isotherm equations, namely, the Langmuir and Freundlich equations (4-5) were used to explore the equilibrium data [39, 40].

$$\frac{c_e}{q_e} = \frac{1}{q_m b} + \frac{c_e}{q_m} \tag{4}$$

$$\log q_e = \log k_f + \frac{1}{n}\log C_e \tag{5}$$

where q_m (mg/g) was the theoretical saturated Cr(VI) adsorption, and b (L/mg) was the Langmuir constant.

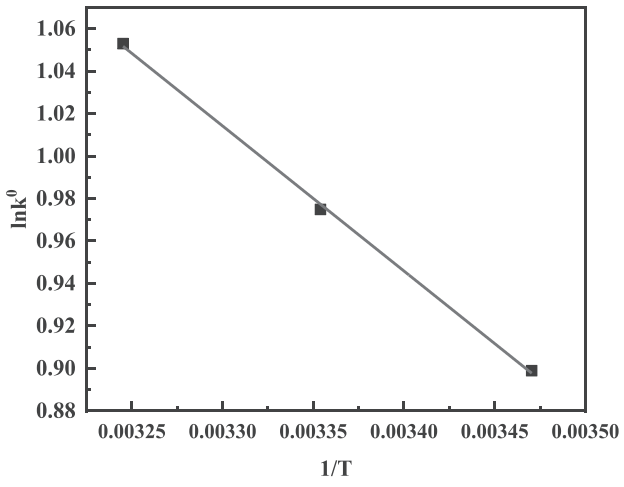

Fig. 7. The relationship between 1/T and lnK0 for the adsorption of Cr(VI) by PGWBC.

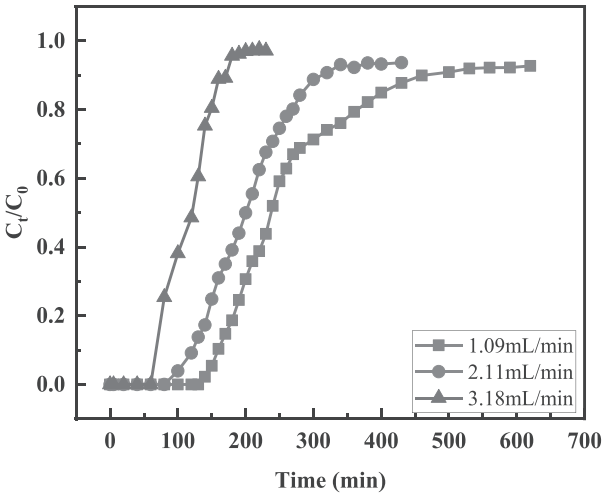

Fig. 8. Penetration curves of Cr(VI) adsorption by PGWBC under three different influent velocities (T=298 K, pH=4, C0=50.2 mg/L).

Both k_f ($L^n \cdot mg^{1-n} \cdot g^{-1}$) and n were the Freundlich constants.

Table 3 showed the isotherm parameters of Cr(VI) by PGWBC at three different temperatures, which indicated that all the three R^2 of the Langmuir model were higher than those of the Freundlich model, indicating the Langmuir model was better at describing the adsorption, and monolayer adsorption of Cr(VI) by PGWBC took place during the process.

Three thermodynamic parameters, including ΔG^0, ΔS^0, and ΔH^0, which were calculated from the following equations (6-8) were used to analyze the thermodynamic feature of Cr(VI) adsorption by PGWBC [41].

$$\Delta G^0 = -RT \ln k \tag{6}$$

$$\Delta G^0 = \Delta H^0 - T\Delta S^0 \tag{7}$$

$$ln\, k = \frac{-\Delta G^0}{RT} = \frac{\Delta S^0}{R} - \frac{\Delta H^0}{RT} \tag{8}$$

where ΔG^0, ΔH^0, and ΔS^0 were the Gibbs free energy change (kJ/mol), the standard enthalpy change (kJ/mol), and the standard entropy change (J/mol·K), respectively. R was the ideal gas constant (8.314 J/mol·K). k was the thermodynamic constant (L/g), which could be calculated from the intercepts of the fitted line shown in Fig. 7.

As shown in Table 4, the ΔG^0 values were all negative and declined with rising temperature, implying that the adsorption of Cr (VI) by PGWBC was a spontaneous process, meanwhile, the positive ΔH^0 and ΔS^0 indicated the endothermic nature of the adsorption process.

Dynamic Adsorption

For further study, the influence of flow rates on Cr(VI) adsorption was investigated by a dynamic adsorption experiment. As shown in Fig. 8, the removal rate and adsorption capacity of PGWBC for Cr(VI) were decreased with the increase of flow rates, meanwhile, the time to reach saturation was also shortened due to the fact that the contact time between Cr(VI) and PGWBC got shorter with the increasing flow rate, leading to the decrease of adsorption capacities [42, 43]. Under the different flow rates of 1.09 mL/min, 2.11 mL/min, and 3.18 mL/min, the maximum Cr(VI) uptakes were 29.53mg/g, 27.76 mg/g, and 23.01 mg/g, respectively, as shown in Table 5.

The Thomas model [44, 45] and Yoon-Nelson model [46, 47] (Eqs. 9-10) were used to fit the maximum adsorption capacity in the dynamic process, the parameters were listed in Table 6 and Table 7.

Table 4. Thermodynamic parameters of adsorption of Cr(VI) by PGWBC.

	T (K)	ΔG^0 (kJ/mol)	ΔH^0 (kJ/mol)	ΔS^0 ($J \cdot mol^{-1} \cdot K^{-1}$)
Cr(VI)	288K	-2.157	5.6815	27.1810
	298K	-2.417		
	308K	-2.698		

Table 5. Dynamic parameters of Cr(VI) adsorption by PGWBC.

Column condition		Breakthrough analysis	
C_0 (mg/L)	Q (mL/min)	R (%)	Q_e (mg/g)
50.22	1.09	43.33	29.53
50.22	2.11	42.43	27.76
50.22	3.18	35.92	23.01

Table 6. Thomas model parameters.

Column condition			Thomas model		
m(g)	C_0 (mg/L)	Q (mL/min)	K_{TH} (mL·min-1·mg-1)	q_0 (mg/g)	R^2
1.00	50.22	1.09	0.22	30.45	0.9850
1.00	50.22	2.11	0.35	27.49	0.9923
1.00	50.22	3.18	0.71	22.27	0.9974

Table 7. Yoon-Nelson model parameters.

Column condition			Yoon-Nelson model			
bed height (cm)	C_0 (mg/L)	Q (mL/min)	K_{YN} (min^{-1})	τ (min)	q_0 (mg/g)	R^2
1.00	50.22	1.09	0.011	279.36	36.48	0.9668
1.00	50.22	2.11	0.018	208.48	34.86	0.9887
1.00	50.22	3.18	0.036	109.37	29.37	0.9059

$$\frac{C_t}{C_0} = \frac{1}{1+\exp\left(\frac{K_{Th}q_0 m}{Q} - K_{Th}C_0 t\right)} \quad (9)$$

$$\frac{C_t}{C_0 - C_t} = \exp\left(K_{YN}t - \tau K_{YN}\right) \quad (10)$$

where C_0 (mg/L) and C_t (mg/L) were the Cr (VI) concentration at initial and time t, q_0 (mg/g) was the theoretical saturated Cr (VI) adsorption uptake, m(g) was the mass of PGWBC, Q (mL/min) was the flow rate, k_{Th} (mL/(min·mg)) was the Thomas constant, K_{YN} (min^{-1}) was the Yoon-Nelson constant, τ (min) was the time required for 50% adsorbent penetration, respectively.

As shown in Table 6, the values of R^2 of Thomas model were higher between the two equations. The theoretical Cr(VI) uptakes calculated from the Thomas equation at varied flow rates were 30.45, 27.49 and 22.27 mg/g, respectively, which agreed with the experimental data, with the maximum relative error being 3.22%. Table 7 showed Cr(VI) uptakes calculated from the Yoon-Nelson equation were 36.48 mg/g, 34.86 mg/g, and 29.37 mg/g, which had the maximum relative error of 22.08% compared with the experimental data. Thus, the Thomas model was more suitable to represent the dynamic Cr(VI) adsorption by PGWBC.

Conclusions

PGWBC prepared under the optimal condition determined in the study was utilized to carry out both static and dynamic Cr(VI) adsorption experiments. The static adsorption experiments revealed that Cr(VI) adsorption by PGWBC decreased from 44.6 mg/g to 3.8 mg/g as the solution pH increased from 2 to 9. The adsorption process fitted the pseudo-second-order model and Langmuir equation well, and had the spontaneous and endothermic nature as well. The results of dynamic adsorption suggested that the maximum Cr(VI) uptakes decreased with the rising flow rate, and the Thomas model was better than the Yoon-Nelson model in representing the dynamic Cr(VI) adsorption by PGWBC.

Acknowledgments

The authors wish to express grateful acknowledgments for the funding support from the Scientific Research Foundation of North China University of Water Resources and Electric Power (No. 40001), and Henan Province Science and Technology Research and Development project (242102231015).

Conflict of Interest

The authors declare no conflict of interest.

References

1. HUANG Y., WANG B., LV J.P., HE Y.N., ZHANG H.C., LI W.Y., LI Y.T., WAGBERG T., HU G.Z. Facile synthesis of sodium lignosulfonate/polyethyleneimine/sodium alginate beads with ultra-high adsorption capacity for Cr(VI) removal from water. Journal of Hazardous Materials, **436**, 129270, **2022**.
2. REN B.Q., JIN Y., ZHAO L.Y., CUI C.W., SONG X.X. Enhanced Cr(VI) adsorption using chemically modified dormant Aspergillus niger spores: Process and mechanisms. Journal of Environmental Chemical Engineering, **10** (1), 106955, **2022**.
3. ASHRAF S., AFZAL M., NAVEED M., SHAHID M., AHMAD ZAHIR Z. Endophytic bacteria enhance remediation of tannery effluent in constructed wetlands vegetated with Leptochloa fusca. International Journal of Phytoremediation, **20**, 121, **2018**.
4. AREGU M.B., ASFAW S.L., KHAN M.M. Developing horizontal subsurface flow constructed wetland using pumice and Chrysopogon zizanioides for tannery wastewater treatment. Environmental Systems Research, **10**, 33, **2021**.
5. ZHAO C., CHEN W. A review for tannery wastewater treatment: some thoughts under stricter discharge requirements. Environmental Science and Pollution Research, **26**, 26102, **2019**.
6. BERHE S., LETA S. Anaerobic co-digestion of tannery waste water and tannery solid waste using two-stage anaerobic sequencing batch reactor: focus on performances of methanogenic step. Journal of Material Cycles and Waste Management, **20**, 1468, **2018**.
7. ASHRAF S., NAVEED M., AFZAL M., SELEIMAN M.F., AL-SUHAIBANI N.A., ZAHIR Z.A., MUSTAFA A., REFAY Y., ALHAMMAD B.A., ASHRAF S. Unveiling the potential of novel macrophytes for the

treatment of tannery effluent in vertical flow pilot constructed wetlands. Water, **12**, 549, **2020**.
8. YOUNAS F., NIAZI N.K., BIBI I., AFZAL M., HUSSAIN K., SHAHID M., ASLAM Z., HUSSAIN M.H., BUNDSCHUH J. Constructed wetlands as a sustainable technology for wastewater treatment with emphasis on chromium-rich tannery wastewater. Journal of Hazardous Materials, **422**, 126926, **2022**.
9. CHANG J.J., ZHANG J., WANG H., BAI Y.F., LIU Y., BI Y.Z., ZHANG H.Z., CHEN H.H., BARNIE S., XIE H.J. Cr(VI) adsorption and reduction by magnetite-humic acid adsorption complexes under mildly acidic conditions: Synergistic/antagonistic mechanism and multi-step reaction model. Chemical Engineering Journal, **451**, 138648, **2023**.
10. XING X., REN X., ALHARBI N.S., CHEN C. Efficient adsorption and reduction of Cr(VI) from aqueous solution by Santa Barbara Amorphous-15 (SBA-15) supported Fe/Ni bimetallic nanoparticles. Journal of Colloid and Interface Science, **629**, 744, **2023**.
11. LI L., ZHANG J., LI Y., YANG C. Removal of Cr(VI) with a spiral wound chitosan nanofiber membrane module via dead-end filtration. Journal of Membrane Science, **544**, 333, **2017**.
12. XU T., ZHOU Y., LEI X., HU B., CHEN H., YU G. Study on highly efficient Cr(VI) removal from wastewater by sinusoidal alternating current coagulation. Journal of Environmental Management, **249**, 109322, **2019**.
13. FYAN L., GUO W.J., HUANG B.B., CHEN Y.J., REN X.Y., SHEN Y.Y., ZHOU Y.F., CHENG R., ZHANG J., QIU M.Q., HU B.W. Efficient removal of Cr (VI) by the modified biochar with chitosan schiff base and $MnFe_2O_4$ nanoparticles: Adsorption and mechanism analysis. Journal of Environmental Chemical Engineering, **11** (2), 109432, **2023**.
14. KARIMI-MALEH H., AYATI A., GHANBARI S., OROOJI Y., TANHAEI B., KARIMI F., ALIZADEH M., ROUHI J., FU L., SILLANPAA M. Recent advances in removal techniques of Cr(VI) toxic ion from aqueous solution: A comprehensive review. Journal of Molecular Liquids, **329**, 115062, **2021**.
15. JIANG R., YAO J., YAO Y. Optimization of The Modified Soybean Straw Activated Carbon for Adsorption of Methylene Blue Dye by Response Surface Methodology. Polish Journal of Environmental Studies, **32** (5), 4073, **2023**.
16. KUMAR A., UPADHYAY S.N., MISHRA P.K., MONDAL M.K. Multivariable modeling, optimization and experimental study of Cr(VI) removal from aqueous solution using peanut shell biochar. Environmental Research, **215**, 114287, **2022**.
17. SHAKYA A., VITHANAGE M., AGARWAL T. Influence of pyrolysis temperature on biochar properties and Cr(VI) adsorption from water with groundnut shell biochars: Mechanistic approach. Environmental Research, **215**, 114243, **2022**.
18. XU D., SUN T., JIA H., SUN Y., ZHU X. The performance and mechanism of Cr(VI) adsorption by biochar derived from Potamogeton crispus at different pyrolysis temperatures. Journal of Analytical and Applied Pyrolysis, **167**, 105662, **2022**.
19. SINGH S., ANIL A.G., NAIK T.S.K., BASAVARAJU U., KHASNABIS S., NATH B., KUMAR V., SUBRAMANIAN S., SINGH J., RAMAMURTHY P.C. Mechanism and kinetics of Cr(VI) adsorption on biochar derived from Citrobacter freundii under different pyrolysis temperatures. Journal of Water Process Engineering, **47**, 102723, **2022**.
20. WANG H., ZHONG D., XU Y., CHANG H., SHEN H., XU C., MOU J.X., ZHONG N. Enhanced removal of Cr(VI) from aqueous solution by nano-zero-valent iron supported by KOH activated sludge-based biochar. Colloids and Surfaces A: Physicochemical and Engineering Aspects, **651**, 129697, **2022**.
21. DENG J., LIU Y., LI H., HUANG Z., QIN X., HUANG J., ZHANG X., LI X.D., LU Q. A novel biochar-copolymer composite for rapid Cr(VI) removal: Adsorption-reduction performance and mechanism. Separation and Purification Technology, **295**, 121275, **2022**.
22. WANG S., WANG X., WANG X., QIN Z., HU J., DING S., FENG K. Study on the Adsorption Behavior of Cadmium by the MPs and Its Environmental Factors. Polish Journal of Environmental Studies, **32** (5), 4313, **2023**.
23. HE Y.N., CHEN J.B., LV J.P., HUANG Y.M., ZHOU S.X., LI W.Y., LI Y.T., ZHANG H.C., WAGBERG T., HU G. Separable amino-functionalized biochar/alginate beads for efficient removal of Cr(VI) from original electroplating wastewater at room temperature. Journal of Cleaner Production, **373**, 133790, **2022**.
24. SAHU S., BISHOYI N., SAHU M.K., PATEL R.K. Investigating the selectivity and interference behavior for detoxification of Cr(VI) using lanthanum phosphate polyaniline nanocomposite via adsorption-reduction mechanism. Chemosphere, **278**, 130507, **2021**.
25. SHI Y., SHAN R., LU L., YUAN H., JIANG H., ZHANG Y., CHEN Y. High-efficiency removal of Cr (VI) by modified biochar derived from glue residue. Journal of Cleaner Production, **254**, 119935, **2020**.
26. JIA P., HUANG Y., CHEN M., QI X., HOU H. Comprehensive evaluation of spent mushroom substrate-chicken manure co-composting by garden waste improvement: physicochemical properties, humification process, and the spectral characteristics of dissolved organic matter. Environmental Science and Pollution Research, **30** (4), 8987, **2023**.
27. ZHANG Q.C., WANG C.C., CHENG J.H., ZHANG C.L., YAO J.J. Removal of Cr(VI) by biochar derived from six kinds of garden wastes: Isotherms and kinetics. Materials, **14** (12), 3243, **2021**.
28. TRUONG H.B., IKE I.A., OK Y.S., HUR J. Polyethyleneimine modification of activated fly ash and biochar for enhanced removal of natural organic matter from water via adsorption. Chemosphere, **243**, 125454, **2020**.
29. HE J, ZHOU H.L., PENG Q.M., WANG Y.T., CHEN Y.J., YAN Z.Y., WANG J.Q. UiO-66 with confined dyes for adsorption and visible-light photocatalytic reduction of aqueous Cr(VI). Inorganic Chemistry Communications, **140**, 109441, **2022**.
30. JIANG B.N., LIN Y.Q., CARLMBOG J. Biochar derived from swine manure digestate and applied on the removals of heavy metals and antibiotics. Bioresource Technology, **270**, 603, **2018**.
31. ZHANG D. Adsorption of Cu^{2+}, Pb^{2+}, Cd^{2+} in Water by Polyethyleneimine Functionalized Straw Biochar. Northeast Normal University, Changchun, China, **2020**.
32. HAFEEZ H.Y., MOHAMMED J., SULEIMAN A.B., NDIKILAR C.E., SAID R.S., MUHAMMAD I. Insights into hybrid TiO_2-g-C_3N_4 heterostructure composite decorated with rGO sheet: A highly efficient photocatalyst for boosted solar fuel (hydrogen) generation. Chemical Physics Impact, **6**, 100157, **2023**.

33. XU J.L., ZHANG D., NIE M.Q., WANG H.X., LI L.W. Adsorption of Cr^{6+} on Polyethyleneimine-functionalized Straw Biochar from Aqueous Solution. Chemical Journal of Chinese Universities, **41** (1), 155, **2020.**
34. THOMBARE N., MAHTO A., SINGH D., CHOWDHURY A.R., ANSARI M.F. Comparative FTIR characterization of various natural gums: A criterion for their identification. Journal of Polymers and the Environment, **31**, 3372, **2023**.
35. LIAN M., MA Y., LI J., SUN J., ZENG X. Influence of pH on the Particulate-Bound Cd Speciation and Uptake by Plants. Polish Journal of Environmental Studies, **31** (6), 5511, **2022**.
36. REVELLAME E.D., FORTELA D.L., SHARP W., HERNANDEZ R., ZAPPI M.E. Adsorption kinetic modeling using pseudo-first order and pseudo-second order rate laws: A review. Cleaner Engineering and Technology, **1**, 100032, **2020**.
37. DEBNATH S., DAS R. Strong adsorption of CV dye by Ni ferrite nanoparticles for waste water purification: Fits well the pseudo second order kinetic and Freundlich isotherm model. Ceramics International, **49** (10), 16199, **2023**.
38. AB GHANI Z., YUSOFF M.S., ALAZAIZA M.Y., AKINBILE C.O., ABD MANAN T.S.B. Landfill leachate treatment by activated carbon (AC) from banana pseudo-stem, iron oxide nanocomposite (IOAC), and iron oxide nanoparticles (IONPs). Journal of Environmental Chemical Engineering, **11** (3), 110132, **2023**.
39. YANG J., SHOJAEI S., SHOJAEI S. Removal of drug and dye from aqueous solutions by graphene oxide: Adsorption studies and chemometrics methods. NPJ Clean Water, **5** (1), 5, **2022**.
40. KALAM S., ABU-KHAMSIN S.A., KAMAL M.S., PATIL S. Surfactant adsorption isotherms: A review. ACS omega, **6** (48), 32342, **2021**.
41. LI H., WANG F., LI J., DENG S., ZHANG S. Adsorption of three pesticides on polyethylene microplastics in aqueous solutions: Kinetics, isotherms, thermodynamics, and molecular dynamics simulation. Chemosphere, **264**, 128556, **2021**.
42. AYDLNA S., NURA H.M., TRAOREA A.M., YLLDLRLMB E., EMIKB S. Fixed bed column adsorption of vanadium from water using amino-functional polymeric adsorbent. Desalination and Water Treatment, **209**, 280, **2021**.
43. HUANG X., HADI P., JOSHI R., ALHAMZANI A.G., HSIAO B.S. A comparative study of mechanism and performance of anionic and cationic dialdehyde nanocelluloses for dye adsorption and separation. ACS omega, **8** (9), 8634, **2023**.
44. LU S., HUANG X., TANG M., PENG Y., WANG S., MAKWARIMBA C.P. Synthesis of N-doped hierarchical porous carbon with excellent toluene adsorption properties and its activation mechanism. Environmental Pollution, **284**, 117113, **2021**.
45. WANG D., CHEN H., ZHANG J., LI J. Easily synthesized mesoporous aluminum phosphate for the enhanced adsorption performance of U(VI) from aqueous solution. Journal of Hazardous Materials, **432**, 128675, **2022**.
46. YU F., YANG Z., ZHANG X., YANG P., MA J. Lanthanum modification κ-carrageenan/sodium alginate dual-network aerogels for efficient adsorption of ciprofloxacin hydrochloride. Environmental Technology & Innovation, **24**, 102052, **2021**.
47. NORDIN A.H., NGADI N., NORDIN M.L., NORALIDIN N.A., NABGAN W., OSMAN A.Y., SHAARI R. Spent tea waste extract as a green modifying agent of chitosan for aspirin adsorption: Fixed-bed column, modeling and toxicity studies. International Journal of Biological Macromolecules, **253**, 126501, **2023**.